Multi-fluid CFD analysis in Process Engineering

IOP Conf. Series: Materials Science and Engineering **276** (2017) 012010 doi:10.1088/1757-899X/276/1/012010

Multi-fluid CFD analysis in Process Engineering

B H Hjertager
Department of Mechanical and Structural Engineering and Materials Science,
University of Stavanger, Stavanger, Norway

E-mail: bjorn.hjertager@uis.no

Abstract. An overview of modelling and simulation of flow processes in gas/particle and gas/liquid systems are presented. Particular emphasis is given to computational fluid dynamics (CFD) models that use the multi-dimensional multi-fluid techniques. Turbulence modelling strategies for gas/particle flows based on the kinetic theory for granular flows are given. Sub models for the interfacial transfer processes and chemical kinetics modelling are presented. Examples are shown for some gas/particle systems including flow and chemical reaction in risers as well as gas/liquid systems including bubble columns and stirred tanks.

1. Introduction

1.1. Basic considerations

Several different approaches are available for setting up the governing equations for multi-phase equipment. One method is the so-called PSIC (Particle-Source-In-Cell) procedure originally presented by Migdal and Agosta [1].This method treats the continuous phase (liquid or gas) in a usual Eulerian description, whereas the dispersed phases (bubbles, droplets or particles) are described in a Lagrangian way. This means that the dispersed phase is tracked through the flow domain from inlet to outlet. In the original method it was assumed no interaction between the various dispersed phases and thus this method was only applicable to low volume fractions of the dispersed phase. In later years this limitation has been removed and the resulting method is called the discrete particle method (DPM).

The second method is the Volume of Fluid (VOF) for gas/liquid systems and was first proposed by Nichols et al. [2]. The method makes it possible to calculate the interphase between the gas and liquid and is thus able to resolve the details of the bubble shapes as they move through the liquid. The method assumes that the flow is fully segregated (resolved), which means that we do not have a mixture of gas and liquid anywhere in the computational cells. We either have pure gas or pure liquid present in the cells. This means that we solve only one set of balance equations: gas or liquid. The inter-phase is tracked by solving a transport equation for the VOF variable. This is a discontinuous variable that is either zero or one. The method is such that in order to resolve sharp interfaces it needs large grid resolution and hence large computer resources.

The third method is the Lattice Boltzman (LB) method that is able to model the flow around solid particles and is therefore able to fully resolve the solids fluid flow. Both the VOF and LB may be characterised by being so-called Direct Numerical Simulation (DNS) method for multi-phase flows.

The fourth method deduces the governing equations based on the Eulerian concept and is normally named the multi-fluid method (Spalding, [3]). This means that the phases are treated as interpenetrating

fluids that share the space and interact through the source terms. All equations are such that the volume fraction may take a value between zero and one.

Figure 1 gives an overview of the four various methods for gas-liquid and gas-solids flow. We note that at the top row in the figure gives the most fundamental methods, i.e. methods that need no modelling since all aspects of the flow are calculated. These methods will however need large computational resources. We also see from the figure that DPM/PSIC approach is an intermediate method where some details are lost and needs to be modelled. The third row in the figure gives the multi-fluid method. This is the most demanding method with regard to modelling needs. The important aspect to note is that due to large dimensions and computing demands the multi-fluid method is the optimum choice for industrial scale process equipment. However, the VOF, LB and DPM/PSIC methods are highly needed to feed better sub-models for the multi-fluid technique. We also see that in the last row it is envisaged a combination of multi-fluid and the DPM methods that may be optimum where large bubbles are flowing through a fluidised bed.

MORE PHYSICS ← SMALL SCALE

Gas liquid flows	Gas solids flows
Interphase tracking, VOF	Lattice Boltzman (LB)
Bubble tracking DPM/PSIC	Particle tracking DPM/PSIC
Multifluid	Multifluid
	Multifluid and bubble tracking

→ MORE MODELING → INDUSTRIAL SCALE

Figure 1: Relations between description level for gas liquid and gas solids systems and 1) degree of modelling details needed and 2) scale of reactor (adapted from van der Hoef et al [4]).

1.2. Objective of the Paper

This paper will mainly deal with the multi-fluid technique. Details will be given on the derivation of the multi-fluid equations. Section II will deal with the basics of the multi-fluid approach. Section III will deal with the closures for bubble-liquid flows whereas Section IV will handle the closure framework for solids fluid flows based on the kinetic theory of granular flow (KTGF). Additional sub models for bubble size, interfacial transfer processes, chemical reaction and stirred tank models are dealt with in Section V. Section VI presents some applications of multi-fluid simulations for bubble columns, stirred tanks and fluidised beds. The final section VII gives a summary of the Paper.

2. Basics of the multi-fluid approach

2.1. Introduction

A multiphase flow system consists of a number of single phase regions bounded by moving interfaces. In principle, a multiphase flow model could be formulated in terms of the local instantaneous variables pertaining to each phase and matching boundary conditions at the interfaces. The direct numerical solution of this kind of formulation is not feasible in practice. It would require an extremely fine mesh and a very small time step. The local instantaneous formulation can be used as starting point to derive macroscopic equations by an average procedure, whose numerical solution is feasible. The modelling of the unclosed terms arising from the average procedures is the price to pay for solving averaged multiphase flow systems.

2.2. Averaged Balance Equations

Multi-fluid model: In cases where a detailed description of the interface dynamics is not relevant or is computationally too expensive, the averaging can be performed on a volume larger than the characteristic volume of the secondary phase as illustrated in Figure2. Doing so, all the information lost on the scales smaller than the averaging scale need to be accounted for through sub-grid models, which may be derived empirically, analytically or numerically. The multi-fluid model is derived from the averaged local instantaneous balance equations with an averaging volume larger than the characteristic volume of the secondary phase, and is based on the assumption of inter-penetrating continuum media. That is, different phases can share the same spatial position.

The multi-fluid model balance equations can be written in a compact form:

Mass balance

$$\frac{\partial}{\partial t}\left(\alpha_k \bar{\rho}_k\right)+\nabla\cdot\left(\alpha_k \bar{\rho}_k \hat{\vec{u}}_k\right)=\Gamma_k \tag{1}$$

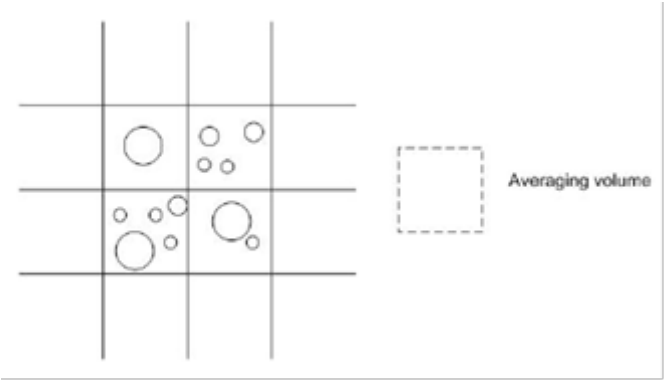

Figure 2: Averaging volume for a multi-fluid flow model framework [13].

Momentum balance

$$\frac{\partial}{\partial t}\left(\alpha_k \bar{\rho}_k \hat{\vec{u}}_k\right)+\nabla\cdot\left(\alpha_k \bar{\rho}_k \hat{\vec{u}}_k \hat{\vec{u}}_k\right)=\nabla\cdot\left[\alpha_k\left(\bar{\bar{T}}_k+\overline{\overline{T_k^t}}\right)\right]+\left(\alpha_k \bar{\rho}_k \vec{g}\right)+\Gamma_k \hat{\vec{u}}_k+\vec{M}_{I,k} \tag{2}$$

Here, Γ_k represents the exchange of mass between phases, $\overline{\overline{T_k^t}}$ is the residual stress tensor accounting for the unresolved turbulence scales and $\vec{M}_{I,k}$ accounts for the interfacial forces.

The following constraints hold

$$\sum_{k=1}^{N}\Gamma_k=0 \quad \text{and} \quad \sum_{k=1}^{N}\alpha_k=1.0 \tag{3}$$

The average energy equation expressed by enthalpy *h* as the dependent variable reads (kinetic energy is subtracted):

$$\frac{\partial}{\partial t}(\alpha_k \bar{\rho}_k \hat{h}_k)+\nabla\cdot(\alpha_k \bar{\rho}_k \hat{\vec{u}}_k \hat{h}_k)=-\nabla\cdot\alpha_k(\hat{\vec{q}}_k+\bar{\bar{q}}_k^t)+\frac{\mathrm{D}_k}{\mathrm{D}t}(\alpha_k p_k) \tag{4}$$

$$+\alpha_k(\hat{\bar{\tau}}_k+\bar{\bar{\tau}}_k^t):\nabla\hat{\vec{u}}_k+\hat{h}_{I,k}\cdot\Gamma_k+\alpha_k\bar{\rho}_k S_k+E_{I,k}$$

Here the terms on the RHS are 1) heat transfer in phase k due to temperature gradients, 2) reversible work in phase k, 3) dissipation due to shear stress in phase k, 4) energy transfer to phase k due to mass transfer between phases, 5) energy generation in phase k due to e.g. chemical reaction and finally 6) heat transfer to phase k from the other phases.

The average balance equation for a chemical specie is expressed as

$$\frac{\partial}{\partial t}(\alpha_k \overline{\rho}_k \overline{Y}_{j,k}) + \nabla \cdot (\alpha_k \overline{\rho}_k \hat{\vec{u}}_k \overline{Y}_{j,k}) = \\ -\nabla \cdot \alpha_k (\overline{\vec{F}}_{Y,k} + \overline{\vec{F}^t}_{Yj,k}) + \overline{Y}_{I,j,k} \cdot \Gamma_k + \alpha_k \overline{\rho}_k \overline{\Psi}_{j,k} \tag{5}$$

Here the terms on the RHS are 1) mass transfer in phase k due concentration gradients, 2) mass transfer to phase k due to mass transfer from the other phases, 3) mass generation of specie Y_j in phase k due to e.g. chemical reaction.

3. Closure framework

3.1. General

So far, all the multiphase models described are not yet in a solvable form. They still include unclosed terms that are not explicitly depending on the averaged fluid properties. Unclosed terms, for multiphase flow models, can be grouped in three different classes:

(i) phase interaction terms $\left(\Gamma_k, \overline{\vec{M}}_{I,k}\right)$,

(ii) self-interaction terms $\left(\overline{\overline{T_k}}\right)$ and

(iii) turbulence terms $\left(\overline{\overline{T_k^t}}\right)$.

Furthermore, the thermodynamic state of the system needs to be specified through state equations, which link the thermodynamic variables. The closures of the terms in (i)-(iii) together with state equations go under the name of closure laws or constitutive laws.

3.2. Bubble Liquid

3.2.1 Self-interaction: The viscous stress tensor of phase k, $\overline{\overline{T}}_k$ can be split up into a pressure term and a shear stress term as

$$\overline{\overline{T}}_k = -p_k \overline{\overline{I}} + \overline{\overline{\tau}}_k \tag{6}$$

The shear stress tensor is often modelled using the Newtonian strain-stress relation

$$\overline{\overline{\tau}}_k = \xi_k \left(\nabla \cdot \hat{\vec{u}}_k\right) \overline{\overline{I}} + 2\mu_k \left[\overline{\overline{S}}_k - \frac{1}{3} \nabla \cdot \hat{\vec{u}}_k \overline{\overline{I}}\right] \tag{7}$$

where the strain-rate tensor is defined by

$$\overline{\overline{S}}_k = \frac{1}{2}\left(\nabla \cdot \hat{\vec{u}}_k + \left(\nabla \cdot \hat{\vec{u}}_k\right)^T\right) \tag{8}$$

The bulk viscosity, ξ_k, is usually set to zero for all phases, whereas the dynamic viscosity, μ_k, is usually set to a constant value (laminar viscosity) for the primary phase (liquid) and to zero for the

secondary phases (classes of bubble). The assumption of constant viscosity for the primary phase may be questionable, since there should be dependence from the concentration of the secondary phases and temperature when non isothermal process is studied. In the present analysis, a constant laminar viscosity is assumed.

3.2.2 Phase interaction: The interactions between the phases are accounted for by the terms $\vec{M}_{I,k}$, Γ_k in the multi-fluid model. The formulation of the exchange mass rate between phases, Γ_k, depends on the particular process under consideration (evaporation, solidification, condensation, etc.) and will not be discussed here.

The interfacial force for phase k is usually decomposed in terms of a generalized drag force and averaged interfacial pressure and shear stress.

$$\vec{M}_{I,k} = \vec{M}^{gd}_{I,k} + p_{I,k}\nabla\alpha_k - \bar{\bar{\tau}}_{I,k}\nabla\alpha_k \tag{9}$$

By this decomposition the RHS of Eq. 2 may be rewritten as follows

$$\begin{aligned}\nabla\cdot\left(\alpha_k\bar{\bar{T}}_k\right)+\left(\alpha_k\bar{\rho}_k\vec{g}\right)+\Gamma_k\hat{\vec{u}}_k+\vec{M}_{I,k} &= -\alpha_k\nabla p_k+\nabla\cdot\left(\alpha_k\bar{\bar{\tau}}_k\right)+\\ +\left(p_{I,k}-p_k\right)\nabla\alpha_k-\bar{\bar{\tau}}_{I,k}\nabla\cdot\alpha_k &+\left(\alpha_k\bar{\rho}_k\vec{g}\right)+\Gamma_k\hat{\vec{u}}_k+\vec{M}^{gd}_{I,k}\end{aligned} \tag{10}$$

The generalized drag force accounts for several interaction forces. Here, only the main contributions for bubbly flows, i.e. drag, virtual mass and lift forces, will be considered. In case of bubbly flows, the multiphase system can be modelled with a primary phase (k=1), consisting of the liquid phase, and (N-1) secondary phases each one representing a class of bubbles with volumes ranging within an interval. Assuming that the interfacial forces are only acting between the primary phase and the secondary phases and not among the secondary phases, which is reasonable for dispersed systems, the generalized drag form can be formulated for the primary phase as

$$\vec{M}^{gd}_{I,1} = \sum_{k=2}^{N}\left(\vec{M}^{D}_{I,k}+\vec{M}^{L}_{I,k}+\vec{M}^{VM}_{I,k}\right) \tag{11}$$

and for the secondary phases as

$$\vec{M}^{gd}_{I,k} = -\vec{M}^{D}_{I,k}-\vec{M}^{L}_{I,k}-\vec{M}^{VM}_{I,k} \qquad k=2,.....N \tag{12}$$

This formulation satisfies the averaged jump constraint for the momentum. The drag, lift and virtual mass are modelled as follows:

Drag force

$$\vec{M}^{D}_{I,k} = \frac{3}{4}\bar{\rho}_1\alpha_k\frac{C_{D,k}}{\bar{d}_{b,k}}\left|\hat{\vec{u}}_k-\hat{\vec{u}}_1\right|\left(\hat{\vec{u}}_k-\hat{\vec{u}}_1\right) \tag{13}$$

Lift force

$$\vec{M}^{L}_{I,k} = -C_{L,k}\bar{\rho}_1\alpha_k\left(\nabla\times\hat{\vec{u}}_1\right)\times\left(\hat{\vec{u}}_k-\hat{\vec{u}}_1\right) \tag{14}$$

Virtual mass force

$$\vec{M}^{VM}_{I,k} = C_{VM,k}\bar{\rho}_1\alpha_k\left(\frac{\mathrm{D}}{\mathrm{D}t}\hat{\vec{u}}_k-\frac{\mathrm{D}}{\mathrm{D}t}\hat{\vec{u}}_1\right)\text{、} \tag{15}$$

3.2.3 Turbulence closure: The averaging process on the convective terms of phase k generates the so called residual stress tensor (or Reynolds stress tensor when a time or ensemble average is performed), $\bar{\bar{T}}^t_k$, which accounts for the residual or unresolved turbulence filtered out by the averaging process. Due to the nature of turbulence, which is still a not well understood problem of physics, the modelling of the residual tensor is not trivial. Kataoka and Serizawa [5] and successively Lopez de Bertodano et al. [6] have derived and extended from single phase to multiphase the k−ε turbulence model. However, in deriving the equations for the turbulent kinetic energy, k, and the turbulent dissipation rate, ε, several cross-correlation terms have been neglected mainly because the lack and the difficulties of understanding them. Hence care must be taken when using this model. The work of Chahed et al. [7] is

one of the few if not the only one in which the Reynolds stress model is applied for multiphase flows. In the last years there has been some attempt to use very large eddy simulations (VLES) for computing multiphase flows, in particular bubbly flows, (Milelli [8], Deen et al. [9], Bove et al. [10]. This technique has shown to be able to capture the unsteadiness and the main characteristic of the flow quite successfully. LES and VLES are based on spatial filtered Navier-Stokes equations. Since the volume average of the multiphase model equations is equivalent to filter in space by a particular filter, they can be regarded as LES/VLES. Here VLES will be considered and the residual stress tensor will be modelled consequently. For the continuous phase, k=1, the residual stress tensor can be written as

$$\overline{\overline{T_1^t}} = \overline{\rho}_1 \left(\hat{\vec{u}}_1 \hat{\vec{u}}_1 - \overline{\vec{u}}_1 \vec{u}_1 \right) = -\frac{2}{3} k_1 \overline{\overline{I}} + \overline{\overline{\tau}}_1 \tag{16}$$

Here, k_1 is the residual turbulent kinetic energy for the continuous phase and is defined as

$$k_1 = \tfrac{1}{2} \overline{\rho}_1 \left(\overline{\vec{u}}_1 \vec{u}_1 - \hat{\vec{u}}_1 \hat{\vec{u}}_1 \right) \tag{17}$$

τ_1 is the anisotropic residual stress tensor and accounts for two different turbulence contributions, one induced by the shear stress in the liquid phase and the other deriving from the bubble liquid interaction or bubble induced turbulence (Sato and Sekoguchi [11]). The linear eddy-viscosity model is used to relate the anisotropic residual stress to the rate of strain and the superposition of the two turbulence effects is assumed. The anisotropic residual stress tensor can then be modelled as

$$\overline{\overline{\tau}}_1 = 2\left(\mu_t + \mu_{t,BIT} \right) \overline{\overline{S}}_1 \tag{18}$$

By analogy with the mixing-length hypothesis, the turbulent viscosity, μ_t, is modelled as (Smagorinsky [12])

$$\mu_t = \overline{\rho}_1 \left(C_s \Delta \right)^2 S_1 \tag{19}$$

where, C_s is the Smagorinsky coefficient, Δ is the filter length or the volume average characteristic length and S_1 is the characteristic filtered rate of strain. It is defined as

$$S_1 = \left(2\overline{\overline{S}}_1 : \overline{\overline{S}}_1 \right)^{1/2} \tag{20}$$

The bubble induced viscosity was introduced and modelled by Sato and Sekoguchi [11] as

$$\mu_{t,BIT} = \overline{\rho}_1 C_{\mu,BIT} \sum_{k=2}^{N} \alpha_k d_k \left| \vec{u}_k - \vec{u}_1 \right| \tag{21}$$

Where the model constant, $C_{\mu,BIT}$, is set equal to 0.6. For the secondary phases, the residual stress tensor should account for the dispersion of the bubbles (or particles in general) due to the unresolved eddies. Bove [13] shows that the modelling of this term by the linear eddy-viscosity assumption is not able to describe the desired physics. Several works account for the turbulent dispersion in the generalized drag force, among others Lopez de Bertodano [14] and Drew and Passman [15]. This is questionable. In fact, if the turbulent dispersion effect is considered in the generalized drag force, what is the meaning of the residual stress tensor for the secondary phases? When VLES is applied to bubbly flows, eddies down to a length scales comparable with the bubble size (two times the bubble diameter if the grid spacing is set equal to the bubble diameter) are resolved. These eddies are responsible of the turbulent dispersion of the gas phase. With an appropriate choice of the grid spacing the most of the turbulent dispersion effect is then resolved and only a small part needs to be modelled. Therefore, the residual stress tensor for the secondary phases will be neglected. The reader can refer to the work of Moraga et al. [16] for a review of various turbulent dispersion models.

Another popular model for bubble liquid flows is to model the continuous phase using the so-called k-ε turbulence model. The dispersed phase influence is taken account by introducing additional source terms. The turbulence viscosity is modelled as

$$\mu_{t,k} = C_\mu \overline{\rho}_k \frac{k_1^2}{\varepsilon_1} \tag{22}$$

The equation for the turbulent kinetic energy for the continuous phase (k=1) reads

$$\frac{\partial}{\partial t}(\alpha\overline{\rho}k)_1+\nabla\cdot(\alpha\overline{\rho}\hat{\vec{u}}k)_1=\nabla\cdot\left(\alpha\frac{\mu_t}{\sigma_k}\nabla k\right)_1+\alpha_1(G+P_{b,k}-\overline{\rho}\varepsilon)_1 \tag{23}$$

The equation for dissipation of turbulent kinetic energy for the continuous phase (k=1) reads

$$\begin{aligned}\frac{\partial}{\partial t}(\alpha\overline{\rho}\varepsilon)_1+\nabla\cdot(\alpha\overline{\rho}\hat{\vec{u}}\varepsilon)_1=\nabla\cdot\left(\alpha\frac{\mu_t}{\sigma_\varepsilon}\nabla\varepsilon\right)_1+\\+\alpha_1\left[\left(\frac{\varepsilon}{k}\left(C_1\,G-C_2\overline{\rho}\varepsilon\right)+P_{b,\varepsilon}\right)\right]_1\end{aligned} \tag{24}$$

Production of turbulence due to mean strain gradients is given by:

$$G_1=\overline{\overline{\tau}}_1:\nabla\hat{\vec{u}}_1 \tag{25}$$

Additional turbulent kinetic energy is produced or dissipated due to the work induced by the bubbles when they move through the liquid phase

$$P_{b,k}=C_b\overrightarrow{M}_1^D\cdot(\hat{\vec{u}}_b-\hat{\vec{u}}_1)\qquad P_{b,\varepsilon}=C_{bd}\,\alpha_g\,\overline{\rho}_1\frac{k_1^{3/2}}{d_b} \tag{26}$$

C_b range from 0.02 to 0.75. This means that from 2 to 75 percent of the bubble-induced turbulence goes into the large eddy structure of the continuous phase. C_{bd} range from 0.02 to 0.2. These large variations in the two constants indicate the problems with the k-ε turbulence model for bubble-liquid flows. The values of the other constants applied in the k-ε model are given in the Table 1 below.

Table 1. Values of constants in the k-ε model

C_μ	C_1	C_2	σ_k	σ_ε
0.09	1.44	1.92	1.0	1.3

Lahey et al. [17] propose an extension to the k-ε model given above. Their extension introduces two time scales, namely one which is the normal turbulent turnover time of the liquid eddies $(k/\varepsilon)_1$ and one which is related to the relative velocity and the bubble diameter ($d_b/|u_{rel}|$). The kinetic energy of turbulence is derived from transport equations, one for shear induced turbulence k_{SI}, and one for bubble induced turbulence k_{BI} . These two contributions are added to get the total turbulent kinetic energy in the liquid phase, k_l.

3.2.4 Closed multi-fluid model: Assuming that the surface tension effect is not important, as it is for non-separated flows, the pressure can be considered to have locally the same value for all phases, $p_k = p_{I,k} = p$. The mass conservation and momentum balance yields

Mass conservation

$$\frac{\partial}{\partial t}\left(\alpha_k\overline{\rho}_k\right)+\nabla\cdot\left(\alpha_k\overline{\rho}_k\hat{\vec{u}}_k\right)=\Gamma_k,\quad k=1,.....,N \tag{27}$$

$$\sum_{k=1}^{N}\alpha_k=1;\quad\sum_{k=1}^{N}\Gamma_k=0 \tag{28}$$

Momentum balance for the primary phase

$$\begin{aligned}
&\frac{\partial}{\partial t}\left(\alpha_1\overline{\rho}_1\hat{\hat{u}}_1\right)+\nabla\cdot\left(\alpha_1\overline{\rho}_1\hat{\hat{u}}_1\hat{\hat{u}}_1\right)=-\alpha_1\nabla p+\alpha_1\overline{\rho}_1\vec{g}+\\
&+\nabla\cdot\left(\alpha_1\mu_{eff,1}\left(\nabla\hat{\hat{u}}_1+\left(\nabla\hat{\hat{u}}_1\right)^T\right)\right)-\nabla\cdot\left(\alpha_1\mu_1\left(\frac{1}{3}\nabla\hat{\hat{u}}_1\overline{\overline{I}}\right)\right)+\\
&+\Gamma_1\hat{\hat{u}}_1+\sum_{k=2}^{N}\frac{3}{4}\overline{\rho}_1\alpha_k\frac{C_{D,k}}{\overline{d}_{b,k}}\left|\hat{\hat{u}}_k-\hat{\hat{u}}_1\right|\left(\hat{\hat{u}}_k-\hat{\hat{u}}_1\right)+\\
&-\sum_{k=2}^{N}C_{L,k}\overline{\rho}_1\alpha_k\left(\nabla\times\hat{\hat{u}}_1\right)\times\left(\hat{\hat{u}}_k-\hat{\hat{u}}_1\right)+\\
&+\sum_{k=2}^{N}C_{VM,k}\overline{\rho}_1\alpha_k\left(\frac{\mathrm{D}}{\mathrm{D}t}\hat{\hat{u}}_k-\frac{\mathrm{D}}{\mathrm{D}t}\hat{\hat{u}}_1\right)
\end{aligned}\tag{29}$$

Here, $\mu_{eff,1}$ represents the sum of the dynamic, μ_1, residual, μ_t, and residual bubble induced viscosity, $\mu_{t,BIT}$.

Momentum balance for the secondary phases

$$\begin{aligned}
&\frac{\partial}{\partial t}\left(\alpha_k\overline{\rho}_k\hat{\hat{u}}_k\right)+\nabla\cdot\left(\alpha_k\overline{\rho}_k\hat{\hat{u}}_k\hat{\hat{u}}_k\right)=-\alpha_k\nabla p+\alpha_k\overline{\rho}_k\vec{g}+\Gamma_1\hat{\hat{u}}_1+\\
&-\frac{3}{4}\overline{\rho}_1\alpha_k\frac{C_{D,k}}{\overline{d}_{b,k}}\left|\hat{\hat{u}}_k-\hat{\hat{u}}_1\right|\left(\hat{\hat{u}}_k-\hat{\hat{u}}_1\right)+\\
&+C_{L,k}\overline{\rho}_1\alpha_k\left(\nabla\times\hat{\hat{u}}_1\right)\times\left(\hat{\hat{u}}_k-\hat{\hat{u}}_1\right)\\
&-C_{VM,k}\overline{\rho}_1\alpha_k\left(\frac{\mathrm{D}}{\mathrm{D}t}\hat{\hat{u}}_k-\frac{\mathrm{D}}{\mathrm{D}t}\hat{\hat{u}}_1\right)\qquad k=2,.....,N
\end{aligned}\tag{30}$$

Normally, the virtual mass coefficient, $C_{VM,k}$, is set equal to 0.5. The lift coefficient, $C_{L,k}$, is either set to a constant value or modelled as suggested by Tomiyama [18],

$$C_{L,k}=\begin{Bmatrix}\min\left[0.288\tanh\left(0.121\cdot\mathrm{Re}\right),\ f\left(Eo\right)\right] & \text{if} & \mathrm{Eo}<4\\ f(Eo) & \text{if} & 4<Eo\end{Bmatrix}\tag{31}$$

where,

$$f\left(Eo\right)=0.00105\cdot Eo^3-0.00159\cdot Eo^2-0.204\cdot Eo+0.474\tag{32}$$

The drag coefficient, $C_{D,k}$, is modelled either by the distorted model (Ishii and Zuber [19])

$$C_{D,k}=\frac{2}{3}Eo_k^{1/2}\tag{33}$$

or by different correlations depending on the mean diameter and the initial deformation of the bubbles as well as the water contamination level, which affects the surface tension (Tomiyama et al. [20], Tomiyama [18]).

For non-contaminated water or high initial shape deformation, the drag coefficient is well correlated by

$$C_{D,k}=\begin{Bmatrix}\frac{16}{\mathrm{Re}_k}\left(1.0+0.15\right)\cdot\mathrm{Re}_k^{0.687} & \text{if} & 0\ mm<\overline{d}_{b,k}<0.5\,mm\\ \frac{48}{\mathrm{Re}_k} & \text{if} & 0.5\ mm<\overline{d}_{b,k}<1.3\,mm\\ \frac{8}{3}\frac{\mathrm{Eo_k}}{\mathrm{Eo_k}+4} & \text{if} & 1.30\ mm<\overline{d}_{b,k}\end{Bmatrix}\tag{34}$$

For contaminated water or low initial shape deformation, the following correlation holds

$$C_{D,k}=\begin{Bmatrix}\frac{16}{\mathrm{Re}_k}\left(1.0+0.15\right)\cdot\mathrm{Re}_k^{0.687} & \text{if} & 0\ mm<\overline{d}_{b,k}<0.8\,mm\\ \text{Correlation} & \text{if} & 0.8\ mm<\overline{d}_{b,k}\end{Bmatrix}\tag{35}$$

Tomiyama [18] expresses the drag coefficient as

$$C_{D,k}=\begin{cases}\dfrac{8}{3}\dfrac{\mathrm{Eo_k}}{ER_k^{2/3}\left(1-ER_k^2\right)^{-1}\mathrm{Eo_k}+16ER_k^{4/3}}\mathrm{F}\left(ER_k\right)^{-2} & \text{if} \quad \mathrm{ER_k}<1.0\\ 6 & \text{if} \quad \mathrm{ER_k}=1.0\\ \dfrac{8}{3}\dfrac{\mathrm{Eo_k}}{ER_k^{2/3}\left(ER_k^2-1\right)^{-1}\mathrm{Eo_k}-16ER_k^{4/3}}G\left(ER_k\right)^{-2} & \text{if} \quad \mathrm{ER_k}>1.0\end{cases} \tag{36}$$

Where,

$$Eo_k=\frac{\Delta\rho g d_{b,k}^2}{\sigma}\quad\left(\text{Eotvos number}\right) \tag{37}$$

$$ER_k=\frac{1}{1+0.163Eo_k^{0.757}}\quad\left(\text{Mean aspect ratio}\right) \tag{38}$$

$$\mathrm{Re}_k=\frac{\rho\left|\vec{u}_{s,kl}\right|\overline{d}_{db,k}}{\mu_1}\quad\left(\text{Bubble Reynolds number}\right) \tag{39}$$

$$F\left(ER_k\right)=\frac{\cos^{-1}ER_k-ER_k\sqrt{1-ER_k^2}}{1-ER_k^2} \tag{40}$$

$$G\left(ER_k\right)=\frac{ER_k\sqrt{ER_k^2-1}-\tanh^{-1}\left(ER_k^{-1}\sqrt{ER_k^2-1}\right)}{ER_k^2-1} \tag{41}$$

The system of Equations (27)-(29) is determined. In fact it has the same number of equations and unknowns. As stated previously, in order to be solved, initial and boundary conditions need to be specified. In general, they depend on the particular type of process to be solved. Therefore, they will be given when the type of flow and its operative environment is known.

4. Closure framework for particle (solids) gas flows

4.1. Kinetic Theory of Granular flow (KTGF) for mono-sized particles

4.1.1 Introduction: Statistical approach used to formulate the constitutive equations of the solid phase equations come from the interactions of the fluctuating motion of the particles with the mean motion of the particles. Such interactions generate stresses in the solids phase and give rise to an effective viscosity of the solids phase. To be able to calculate these stresses and an effective solids viscosity, a model is proposed by Ding and Gidaspow [21] and Gidaspow [22]. The model is based on the kinetic theory of dense gases, as presented by Chapman and Cowling [23] and the work of Jenkins and Savage [24] and Lun et al. [25].The thermal temperature in the kinetic theory of dense gases is here replaced with a granular temperature for which a transient differential equation is derived. The solid viscosity and solid stresses are a function of this granular temperature that varies with time and space in a fluidized bed. Derivation given is mainly based on the work of Gidaspow [22]. The generalised model for multi-sized particles given by Manger [26] will be summarized below.

In gas/solid systems, particle segregation due to different size and/or density will play a significant role on the flow behaviour. To describe such phenomena, an extension to multiple particle phases is essential. Jenkins and Mancini [27] extended the kinetic theory for granular flow to binary mixtures. The basic assumption was equal turbulent kinetic energy with a small correction for the individual phase temperatures. Mathiesen et al. [28] developed a model based on this work and performed a simulation with one gas and three solid phases. The model predicted segregation effects fairly well, and good

agreement with experimental data was obtained. Gidaspow et al. [29] and Manger [26] extended the kinetic theory to binary mixtures of solid with unequal granular temperatures between the phases. Based on their research, a generalized multiphase gas/solid model will be given in the next section.

4.1.2 Summary of Governing Equations for Fluid/Multi-sized particle flows: The three-dimensional, finite-volume, multiphase Eulerian/Eulerian CFD code FLOTRACS-MP- 3D (see also Mathiesen et al., [30] [31], Ibsen et al., [32] and Hansen et al. [33]) uses the generalized fluid/multi-sized particle model mentioned above. The turbulent motion of the particulate phase is modelled using the kinetic theory of granular flow described by Manger [26] and the gas phase turbulence is modelled using a LES/Sub-Grid-Scale model.

4.1.3 Mass balances and momentum balances: The governing equations may be written as:

Continuity equation for phase k without mass transfer:

$$\frac{\partial}{\partial t}\left(\alpha_k \rho_k\right) + \frac{\partial}{\partial x_i}\left(\alpha_k \rho_k U_{i,k}\right) = 0 \tag{42}$$

Here α, ρ and U are the volume fraction, density and velocity of phase k, respectively. The momentum equation for phase k is written as:

$$\frac{\partial}{\partial t}\left(\alpha_k \rho_k U_{j,k}\right) + \frac{\partial}{\partial x_i}\left(\alpha_k \rho_k U_{i,k} U_{j,k}\right) = -\alpha_k \frac{\partial p}{\partial x_j} + \frac{\partial}{\partial x_i}\tau_{ij,k} + \alpha_k \rho_k g_j + \sum_{m=1, m\neq k}^{M} \beta_{km}\left(U_{j,m} - U_{j,k}\right) \tag{43}$$

Here p, τ_{ij}, g and β are pressure, stress tensor, gravity and the inter-phase drag coefficient, respectively. There are N solids phases (s) and one gas phase (g) and the total number of phases are therefore M = N+1.

4.1.4 Auxiliary relations: The gas phase stress tensor is given by:

$$\tau_{ij,g} = \mu_{eff,g}\left[\left(\frac{\partial U_j}{\partial x_j} + \frac{\partial U_i}{\partial x_j}\right) - \frac{2}{3}\delta_{ij}\frac{\partial U_k}{\partial x_k}\right]_g \tag{44}$$

where δ_{ij} is the Kroenecker delta. The effective viscosity, $\mu_{eff,g}$, is derived from a sub-grid-scale (SGS) model based on Smagorinsky [12], where the effective viscosity is a sum of a laminar and a turbulent part.

$$\mu_{eff,g} = \alpha_g\left(\mu_{lam,g} + \mu_{turb,g}\right) = \alpha_g \mu_{lam,g} + \alpha_g \rho_g \left(c_t \Delta\right)^2 \sqrt{S_{ij,g} : S_{ij,g}} \tag{45}$$

The SGS eddy coefficient, c_t, is set to 0.079 based on Deardoff [34]. The length scale, Δ, and the strain rate tensor of the resolved field, $S_{ij,g}$, are given by:

$$\Delta = \left(\Delta x \Delta y \Delta z\right)^{1/3} \text{ and}$$

$$S_{ij,g} = \frac{1}{2}\left[\frac{\partial U_j}{\partial x_i} + \frac{\partial U_i}{\partial x_j}\right]_g \tag{46}$$

The solid phase stress tensor is given by:

$$\tau_{ij,s} = -P_s\delta_{ij} + \xi_s\delta_{ij}\frac{\partial U_{k,s}}{\partial x_k} + \mu_s\left[\left(\frac{\partial U_j}{\partial x_i} + \frac{\partial U_i}{\partial x_j}\right) - \frac{2}{3}\delta_{ij}\frac{\partial U_k}{\partial x_k}\right]_s \tag{47}$$

The solids phase pressure, P_s, the bulk viscosity, ξ_s, and the shear viscosity, μ_s, are derived from the kinetic theory of granular flow. The solids pressure is found from, Ding and Gidaspow [21]:

$$P_s = \sum_{n=1}^{N} P_{C,sn} + \alpha_s\rho_s\Theta_s \tag{48}$$

where $P_{C,n}$ is the pressure caused by collisions between the solids phases s and n and has the expression:

$$P_{C,sn} = \frac{\pi}{3}(1+e_{sn})d_{sn}^3 g_{sn} n_s n_n \left[\frac{m_0\theta_s\theta_n}{(m_s/m_n)\theta_s + (m_n/m_s)\theta_n}\right]\cdot\left[\frac{(m_0/m_s)^2\theta_s\theta_n}{\left(\theta_s + (m_s/m_n)^2\theta_n\right)(\theta_s+\theta_n)}\right]^{3/2}$$

$$e_{sn} = \frac{1}{2}(e_n + e_s), \quad d_{sn} = \frac{1}{2}(d_n + d_s) \quad \text{and} \quad m_0 = m_s + m_n \tag{49}$$

where *e, d, n* and m are coefficient of restitution, diameter of the particle, number of particles and mass of a particle, respectively. The coefficient of restitution is unity for fully elastic, and zero for inelastic collisions. By using the assumption of spherical particles, number of particles and mass of a particle are, respectively:

$$n_s = \frac{6\alpha_s}{\pi d_s^3} \quad \text{and} \quad m_s = \frac{\pi d_s^3\rho_s}{6} \tag{50}$$

where g_{sn} is the radial distribution function, which is close to one for dilute flow and approach infinity for dense flow making motion impossible. Based on the single solid phase model given implicitly by Bagnold [35], a new binary radial distribution function is proposed here:

$$g_0 = \left[1 - \left(\frac{\alpha_s}{\alpha_{s,\max}}\right)^{1/3}\right]^{-1} \qquad g_{sn} = \frac{N}{2}\frac{g_0}{1-\alpha_g}(\alpha_s + \alpha_n) \tag{51}$$

The maximum solids packing, $\alpha_{s,max}$, is often put to 0.65. The solids bulk viscosity is calculated as (Ding and Gidaspow, [21]):

$$\xi_s = \sum_{n=1}^{N} P_{C,sn}\frac{d_{sn}}{3}\left(\theta_s + (m_n/m_s)\theta_n\right)\sqrt{\frac{2}{\pi\theta_s\theta_n\left(\theta_s + (m_n/m_s)^2\theta_n\right)}} \tag{52}$$

The solids phase shear viscosity consists of a kinetic term:

$$\mu_{col,s} = \sum_{n=1}^{N} P_{C,sn}\frac{d_{sn}}{3}\left(\theta_s + (m_n/m_s)\theta_n\right)\sqrt{\frac{2}{\pi\theta_s\theta_n\left(\theta_s + (m_n/m_s)^2\theta_n\right)}} \tag{53}$$

and a collisional part:

$$\mu_{kin,s} = \frac{2\mu_{dil,s}}{\frac{1}{N}\sum_{n=1}^{N}(1+e_{sn})g_{sn}}\left[1 + \frac{4}{5}\sum_{n=1}^{N} g_{sn}\alpha_n(1+e_{sn})\right]^2 \tag{54}$$

where the dilute solids viscosity, $\mu_{dil,s}$, is found from:

$$\mu_{dil,s} = \frac{15}{8d_s^3}\alpha_s l_s\sqrt{\frac{2m_s\theta_{s,av}}{\pi}} \text{ and } l_s = \frac{1}{6\sqrt{2}}\frac{d_s}{\alpha_s} \tag{55}$$

To ensure that the dilute viscosity is finite as the volume fraction of solid approaches zero, the mean free path l_s is limited by a characteristic dimension. The average granular temperature $\theta_{s,av}$ is obtained from:

$$\theta_{s,av} = \frac{2m_s\theta_s}{\left[\sum_{n=1}^{N}\frac{n_n}{n_s}\left(\frac{d_{sn}}{d_s}\right)^2\sqrt{\frac{\left(m_0/m_s\right)^2\theta_n}{\left(\theta_s+\left(m_0/m_s\right)^2\theta_n\right)}}S^{3/2}\right]^2} \qquad (56)$$

$$S = \frac{\left(m_0/m_s\right)^2\theta_s\theta_n}{\left(\theta_s+\left(m_0/m_s\right)^2\theta_n\right)\left(\theta_s+\theta_n\right)}$$

Three solids gas inter-phase drag models will be presented.

Model 1 Gidaspow [22]: For $\alpha_g \leq 0.8$ the inter-phase drag coefficient is found from the Ergun equation (Ergun, [36]):

$$\beta_{sg} = 150\frac{\alpha_s^2\mu_{lam,g}}{\alpha_g\left(\Phi_s d_s\right)^2} + 1.75\frac{\alpha_s\rho_g\left|\vec{u}_g-\vec{u}_s\right|}{\Phi_s d_s} \qquad (57)$$

where Φ_s is the sphericity of the particles (i.e. 1.0 for spheres; 0.81 for cubes; 0.6 - 0.7 for crushed materials; 0.3 for Raschig rings).

For $\alpha_g > 0.8$ the drag formulation of Wen and Yu [37] is used

$$\beta_{sg} = \frac{3}{4}C_D\frac{\alpha_s\alpha_g\rho_g\left|\vec{u}_g-\vec{u}_s\right|}{\phi_s d_s}\alpha_g^{-2.65} \qquad (58)$$

with a drag coefficient, C_D, from Rowe [38]:

$$C_D = \begin{cases}\frac{24}{\mathrm{Re}_s}\left(1+0.15\,\mathrm{Re}^{0.687}\right) & \text{for} \quad \mathrm{Re}_s \leq 1000\\ 0.44 & \text{for} \quad \mathrm{Re}_s > 1000\end{cases} \qquad (59)$$

where the particle Reynolds number is defined as:

$$\mathrm{Re}_s = \frac{d_s\rho_g\alpha_g\left|\vec{u}_g-\vec{u}_s\right|}{\mu_{lam,g}} \qquad (60)$$

Model 2 Gibilaro et al. [39]:

$$\beta_{sg} = \left(\frac{17.3}{\mathrm{Re}_p}+0.336\right)\frac{\rho_g}{d_p}\left|\vec{u}_g-\vec{u}_s\right|\alpha_s\alpha_g^{-1.8} \qquad (61)$$

Model 3 Syamlal and O'Brien [40]:

$$\beta_{sg} = \frac{3}{4d_p}C_D\rho_g\frac{1}{R_t^2}\alpha_g\left(1-\alpha_g\right)\left|\vec{u}_g-\vec{u}_s\right| \qquad (62)$$

R_t is the ratio between the falling velocity of a suspension and the terminal velocity of a single sphere. R_t, C_D, A and B are given by the following expressions:

$$2R_t = A - 0.06\,\mathrm{Re}_p + \sqrt{0.0036\,\mathrm{Re}_p^2 + 0.12\,\mathrm{Re}_p\left(2B - A\right) + A^2}$$
$$A = \alpha_g^{4.14} \qquad B = \begin{cases} 0.8\alpha_g^{-1.28} & \text{for } \alpha_g < 0.85 \\ \alpha_g^{2.65} & \text{for } \alpha_g > 0.85 \end{cases}$$
$$C_D = \left(0.63 + 4.8\sqrt{\frac{R_t}{\mathrm{Re}_p}}\right) \qquad \mathrm{Re}_p = \frac{d_s \rho_g \left|\vec{u}_g - \vec{u}_s\right|}{\mu_{lam,g}} \tag{63}$$

The particle/particle drag coefficient may be expressed as (Manger [26]):

$$\beta_{s,g} = P_{C,sn}\left[\begin{array}{l} \dfrac{3}{d_{sn}}\sqrt{\dfrac{2\left(m_s^2\theta_s + m_n^2\theta_n\right)}{\pi m_0^2 \theta_s \theta_n}} + \\ + \dfrac{1}{\left|\vec{u}_n - \vec{u}_s\right|}\left(\nabla\left|\ln\dfrac{\alpha_s}{\alpha_n}\right| + \dfrac{\theta_s\theta_n}{\theta_s + \theta_n}\left|\dfrac{\nabla\theta_n}{\theta_n^2} - \dfrac{\nabla\theta_s}{\theta_s^2}\right| + 3\nabla\left|\dfrac{\ln\left(m_n\theta_n\right)}{\ln\left(m_s\theta_s\right)}\right|\right) \end{array}\right] \tag{64}$$

4.1.5 Granular temperature: A transport equation for the solids phases' turbulent kinetic energy or granular temperature is solved:

$$\frac{3}{2}\left[\frac{\partial}{\partial t}\left(\alpha_s\rho_s\theta_s\right) + \frac{\partial}{\partial x_i}\left(\alpha_s\rho_s U_{i,s}\theta_s\right)\right] = \frac{\partial}{\partial x_i}\left(\kappa_s\frac{\partial\theta_s}{\partial x_i}\right) + \\ + \tau_{ij,s} : \frac{\partial U_{j,s}}{\partial x_i} - \gamma_s - 3\beta_{sg}\theta_s \tag{65}$$

Here, the terms on the right side of the equation represent diffusive transport, production due to shear, dissipation due to inelastic collisions and dissipation due to fluid friction. The dissipation due to inelastic collisions is given by Manger [26].The production/dissipation term due to fluctuations in drag has been assumed as negligible. This is a reasonable assumption for the relatively large and heavy particles. Hence, the particle response time is assumed much longer than the characteristic time scale for the turbulent fluid motion.

The conductivity of granular temperature κ_s, and the dissipation due to inelastic collisions γ_s are determined from the kinetic theory for granular flow [26]. The conductivity is given by a dilute and a dense part as:

$$\kappa_s = \frac{2\kappa_{dil,s}}{\frac{1}{N}\sum_{n=1}^{N}\left(1+e_{sn}\right)g_{sn}}\left(1 + \frac{6}{5}\frac{1}{N}\sum_{n=1}^{N}\left(1+e_{sn}\right)g_{sn}\alpha_n\right)^2 + \\ + 2\alpha_s^2\rho_s d_s\sqrt{\frac{\theta_s}{\pi}}\sum_{n=1}^{N}\left(1+e_{sn}\right)g_{sn}\alpha_n \tag{66}$$

where

$$\kappa_{dil,s} = \frac{225}{32}\alpha_s l_s\sqrt{\frac{2m_s\theta_{s,av}}{\pi}}$$

The dissipation due to inelastic collisions is given by (Manger [26]):

$$\gamma_s = \sum_{n=1}^{N}\frac{3}{4}P_{C,sn}\frac{1-e_{sn}}{d_{sn}}\cdot \\ \cdot\left[4\sqrt{\frac{2\theta_s\theta_n}{\pi\left(\left(m_s/m_0\right)^2\theta_s + \left(m_n/m_0\right)^2\theta_n\right)}} - d_{sn}\left(\frac{\left(m_s/m_0\right)\theta_s + \left(m_n/m_0\right)^2\theta_n}{\left(m_s/m_0\right)^2\theta_s + \left(m_n/m_0\right)^2\theta_n}\right)\frac{\partial U_{k,s}}{\partial x_k}\right] \tag{67}$$

The divergence term is often neglected. However, if the term is retained it may cause production instead of dissipation, and must be handled with special care.

5. Additional sub models

5.1. Bubble Size Models

Five different bubble size models are examined. These are denoted models A to E.

Model A: The simplest model assumes that the bubble size is constant and given by overall flow conditions. Johansen and Boyson [41] have used an estimation of the bubble diameter which is dependant on the inlet flow rate:

$$d_b = 0.35\left(\frac{\dot{V}_g}{g}\right)^{0.2} \tag{68}$$

Model B: Jakobsen [42] has used a bubble size model which sets the diameter proportional to the length scale of the turbulent liquid eddies according to:

$$d_b = C_{SMD}\frac{k_l^{\frac{3}{2}}}{\varepsilon_l} \tag{69}$$

The constant C_{SMD} is determined to be 0.04 for flow in bubble columns. The two models given above do not include properties of the interface. This is included in the next model.

Model C: Calderbank [43] has proposed an expression based on dissipation length scale and a critical Weber number as follows:

$$We_{crit} = \frac{\tau\, d_b}{\sigma};\ \tau = \rho_l\, u_{t,l}^2\ ;\ \varepsilon_l = \frac{u_{t,l}^3}{d_b} \tag{70}$$

Here τ is the shear stress, $u_{t,l}$ is the turbulence velocity, σ is the surface tension of the gas liquid interface and ε is the dissipation rate of turbulence. The expression for d_b from the above relations gives:

$$d_b = C_{We}\left(\frac{\sigma}{\rho_l}\right)^{0.6}\frac{1.0}{\varepsilon_l^{0.4}} \tag{71}$$

Experimental verification against data from stirred tanks has given the following correlation based on the above expression:

$$d_b = C_{We}\left(\frac{\sigma}{\rho_l}\right)^{0.6}\frac{1}{\varepsilon_l^{0.4}}\alpha_g^{0.5}\left(\frac{\mu_g}{\mu}\right)^{0.25} + 0.0009 \tag{72}$$

When C_{We} is taken to be 4.15, d_b is given in metres.

Model D: Both models B and C give bubble size as function of local properties. However, in many cases history effects govern the bubble size. Cook and Harlow [44] give a model that takes account of this. This model calculates the transport of the number concentration of bubbles N, according to:

$$\frac{\partial N}{\partial t} + \nabla\cdot(\vec{u}_g\, N) = \omega_b(N_e - N) \tag{73}$$

Here the equilibrium number concentration of bubbles N_e, is calculated based on a critical Weber number as:

$$N_e = \frac{6\,\alpha_g}{\pi\, d_{be}^3} \quad \text{with} \quad We_{crit} = \frac{(\rho_l - \rho_g)|\vec{u}_{rel}|^2\, d_{be}}{\sigma} \tag{74}$$

The bubble diameter relates to the void fraction and the bubble number concentration as:

$$d_b = \left(\frac{6\,\alpha_g}{\pi\, N}\right)^{\frac{1}{3}} \tag{75}$$

The two constants in the model, the critical Weber number We_{crit}, and the relaxation parameter ω_b, has the following values: 3.6 and between 4 and 20, respectively. These constants are determined for vertical gas-liquid flow past an obstacle.

Model E: The most general and comprehensive method is to calculate bubble size distribution by solving the Population Balance Equation. Here there are several methods available including: Classes/Sectional Methods (CM/SM) and methods of moments (QMOM, DQMOM, PPDC). Details of these methods will not be discussed here but a full description may be found in Bove [14] and Marchisio and Fox [45].

5.2. Interfacial Heat Transfer

Gas/liquid: Heat transfer between the two phases without mass transfer may be treated as follows:

T_1 and T_2 are the temperatures in the bulk of phase 1 and 2, respectively. T_s is the interface temperature. Energy balance over the phase separation surface: heat in = heat out.

$$Q_{1s} = (\lambda_1 a)(T_1 - T_s); \quad Q_{s2} = (\lambda_2 a)(T_s - T_2)$$

Solving for T_s , $Q_{1s} = Q_{2s}$

$$Q_{1s} = Q_{12} = a\frac{\lambda_1\lambda_2(T_1 - T_2)}{\lambda_1 + \lambda_2}$$

Or as source term in the phase 2 and phase 1 enthalpy equations reads:

$$S_{h_2} = -S_{h_1} = aU(T_1 - T_2) \text{ where } \quad 1/U = 1/\lambda_1 + 1/\lambda_2 \tag{76}$$

Here U is the total heat transfer coefficient between phase 1 and 2; λ_1 and λ_2 are the individual heat transfer coefficients between phase 1 and the interface and phase 2 and the interface, respectively; a is the specific surface area of the interface, i.e. area per unit volume.

Gas/particle: Heat may be generated by the catalytic exothermic solid phase chemical reaction [46]. This heat is transported between the phases (particles, p and gas, g) and may in addition be cooled by e.g. generation of steam in a submerged heat exchanger (wall, w).

Source term for the gas phase

$$S_{h_g} = h_v(T_p - T_g) + h_w(T_w - T_g) \tag{77}$$

Source term for the solids phase

$$S_{h_p} = h_v(T_g - T_p) + h_w(T_w - T_p) + \sum_{k=1}^{k=nreac} \Delta H_{rx,k} \cdot r_k \tag{78}$$

The effective transport coefficients relates to the turbulent viscosities as:

$$\Gamma_{h,g} = \frac{\kappa_{lam,g}}{c_{p,g}} + \frac{\mu_g}{0.7} \quad \text{and} \quad \Gamma_{h,p} = \frac{\mu_p}{0.7} \tag{79}$$

Where $\kappa_{lam,g}$ is the laminar conductivity and $c_{p,g}$ is the specific heat capacity of the gas.

The volumetric heat transfer coefficient h_v may be calculated by using several different correlations for the Nusselt number N_p in different flow regimes, characterized by the Reynolds number Re and the gas phase volume fraction α_g.

For $\alpha_g \leq 0.8$

$$\begin{aligned} N_p &= (2 + 0.106\,Re)\,S_p; && Re \leq 200 \\ N_p &= 0.123\left(\frac{4\,Re}{d_p}\right)^{0.83} S_p^{0.17}; && 200 < Re \leq 2000 \\ N_p &= 0.61\,Re^{0.67}\,S_p; && Re > 2000 \end{aligned} \tag{80}$$

For $\alpha_g > 0.8$

$$\begin{aligned} N_p &= (2 + 0.16\, Re^{0.67})\, S_p; \qquad Re \le 200 \\ N_p &= 8.2\, Re^{0.60}\, S_p; \quad 200 < Re < 1000 \\ N_p &= 1.06\, Re^{0.457}\, S_p; \quad Re \ge 1000 \end{aligned} \tag{81}$$

where

$$Re = \frac{\rho_g\, d_p\, |\vec{u}_g - \vec{u}_p|}{\mu_{lam,g}}\ ,\ S_p = \frac{\alpha_p\ 6}{d_p}\ ,\ N_p = \frac{h_v\, d_p}{\kappa_{lam,g}} \tag{82}$$

The wall to bed heat transfer coefficient, h_w, may for many cases be taken to be a constant, only proportional to the respective volume fractions of the phases. Typical values for the bed to wall heat transfer coefficient may be found in Geldart [47].

5.3. Mass Transfer in Bubble Liquid Flows

The interface mass transfer driven by concentration gradients is taken account of through the source terms for the species equation. For the liquid phase, $Y_{j,l}$, the source term reads:

$$S_{Y\,jl} = (k_l a)_l\ (Y_{j,g} - Y^*_{j,l}) \tag{83}$$

The $(k_l\, a)$ is related to the dissipation rate, ε_l gas fraction, α_g and bubble diameter, d_b (Trägårdh, [48]):

$$(k_l a) = C_m \varepsilon_l^{0.2} \frac{6\, \alpha_g}{d_b} \tag{84}$$

Modelling of mass transfer in single component two-phase flow where evaporation/condensation occurs, may be expressed as:

$$\Gamma = \frac{(\lambda_1 a)(T_1 - T_{1s}) + (\lambda_2 a)(T_2 - T_{2s})}{h_{12}} \tag{85}$$

Here T_{1s} and T_{2s} are saturation temperatures, dependant only on pressure; λ_1 is the heat transfer coefficient between phase 1 and the interface surface. λ_2 is the heat transfer coefficient between phase 2 and the interface surface, h_{12} enthalpy of evaporation and a specific surface area of interface.

5.4. Chemical Reaction

Catalytic reaction

The ozone decomposition reaction: The ozone decomposition reaction is a simple irreversible first order catalytic reaction. The reaction can be written as:

$$2\ O_3 \rightarrow 3\ O_2$$

Due to the low concentration of ozone in a riser, the heat produced by the chemical reaction is negligible and the reaction is looked upon as being isothermal.

Species conservation equations: A transport equation for the mass fraction of ozone in the gas phase $Y_{k,g}$ is solved

$$\frac{\partial}{\partial t}(\alpha \rho Y_k)_g + \frac{\partial}{\partial x_i}(\alpha \rho U_i Y_k)_g = \frac{\partial}{\partial x_i}\left[\Gamma_{Y_{k,g}} \frac{\partial Y_k}{\partial x_i}\right] + \alpha_g \cdot r \tag{86}$$

where the transport coefficient Γ_Y is expressed in terms of the diffusion coefficient, D_Y, and the turbulent viscosity of the gas phase:

$$\Gamma_{Y_{k,g}} = D_{Y_{k,g}} + \frac{\mu_{turb,g}}{0.7} \tag{87}$$

The reaction rate constant for the catalytic reaction was measured in a fixed bed reactor. The rate constant is expressed pr. unit volume of catalyst and was measured to be 3.96 s^{-1} (Ouyang et al., [49]). The reaction rate is expressed as:

$$r = -3.96 \cdot \alpha_s \cdot C_{Ozone} \qquad [\text{kg Ozone/m}^3\ \text{s}] \tag{88}$$

6. Applications

The next subsections will give some examples of use of some of the models described above.

6.1. Bubble Columns

In the work of Deen et al. [9] the use of large eddy simulations (LES) in numerical simulations of the gas–liquid flow in bubble columns was studied. The Euler–Euler approach was used to describe the equations of motion of the two-phase flow. It was found that, when the drag, lift and virtual mass forces are used, the transient behaviour that was observed in experiments can be captured. Good quantitative agreement with experimental data is obtained both for the mean velocities and the fluctuating velocities (Figure 3). The LES showed better agreement with the experimental data than simulations using the k–ε model.

Bove [13] extended the above modelling by including solution of the Bubble population equation using three nodes in the size coordinate. This enabled calculation of the bubble size distribution in bubble columns. An example of Bove's results are given in Figure 4.

.

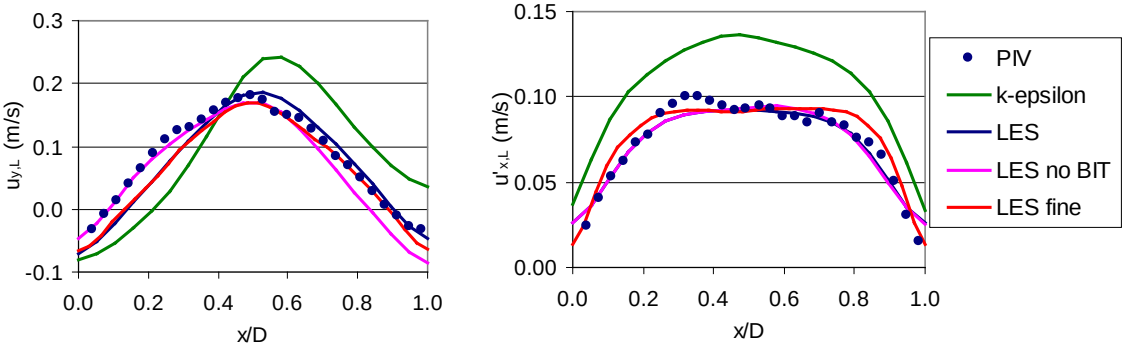

Figure 3: Comparison of simulated and experimental profiles of (left) the axial average liquid velocity and (right) the transverse liquid velocity fluctuations for different conditions.

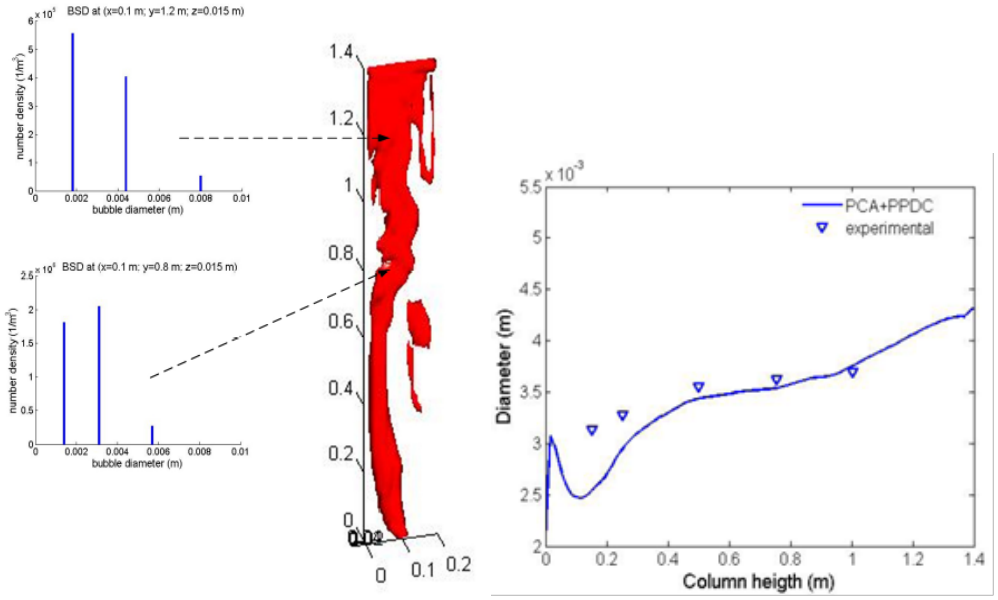

Figure 4: (left) A snap shot of the predicted size distribution at two position in the bubble column of van den Hengel et al [50] and (right) the predicted and measured bubble diameter along the column centreline.

6.2. Stirred Tanks

Deen et al [51] did a study of flow in a stirred tank. A two-camera PIV technique was used to obtain angle resolved velocity and turbulence data of the flow in a lab-scale stirred tank, equipped with a Rushton turbine

Two cases were investigated: a single-phase flow and a gas-liquid flow. In the former case, the classical radial jet flow pattern accompanied by two trailing vortices was observed. In the latter case, the velocity of the radial jet was reduced, and the vortices were diminished by the presence of the gas. Gas cavities clinging to the back of the impeller blades were observed (Figure 5). Both cases were also investigated with the use of three-dimensional transient CFD simulations. The sliding grid technique was used to describe the movement of the impeller.

For the single-phase flow the simulations in the impeller region corresponded very well with the experimental data. For the gas-liquid flow both the mean and fluctuating liquid velocities in the impeller region were well predicted as seen in Figure 6. This was also the case for the mean radial gas velocities. The largest differences between the simulations and the experiments were found for the mean axial gas velocity.

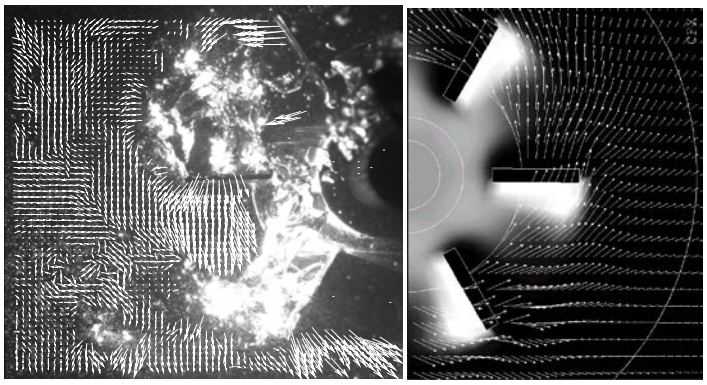

Figure 5: Comparisons between measured (left) and computed (right) distribution of gas around the impeller.

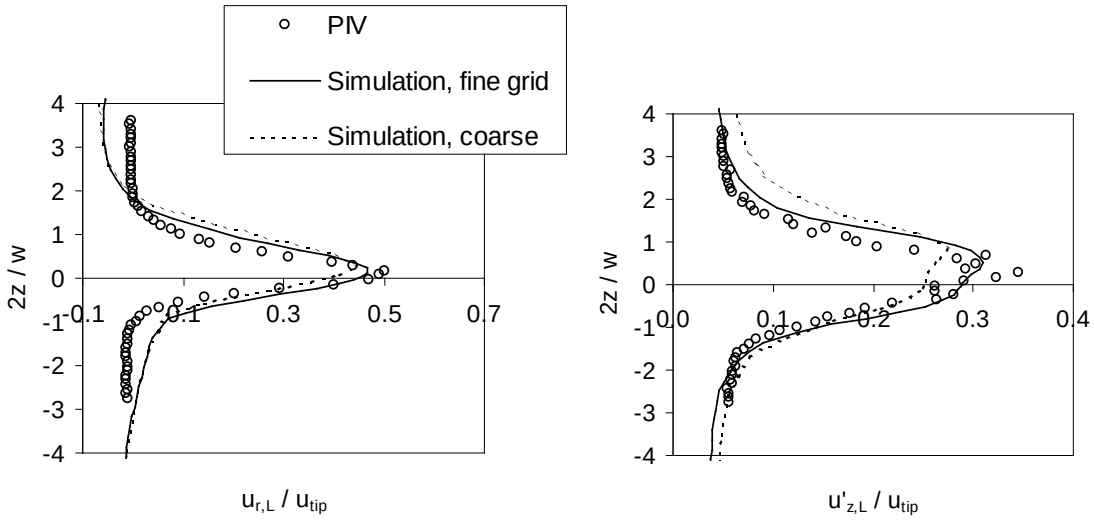

Figure 6: Comparisons of measured and predicted radial liquid velocity (left) and axial liquid turbulent velocity (right) close to the impeller region. The gas liquid case using fine or coarse grids.

6.3. Circulating fluidized beds

6.3.1 Cold flow: Hansen et al [33] have performed a computational fluid dynamics simulation of a cold flowing riser fluidized with FCC catalysts. The computations were performed using the 3D multiphase computational fluid dynamics code with an Eulerian description of both gas and particle phase, described above. The turbulent motion of the particulate phase was modeled using the kinetic theory for granular flow, and the gas phase turbulence was modeled using a Sub-Grid-Scale model. The complex inlet geometry was approximated using multiple inlet patches. The first results were submitted to a blind-test in connection to the 10th international workshop on two-phase flow prediction held in Merseburg, Germany, 2002.

The results were subsequently validated against experimental findings of particle mass flux across the riser and pressure profile along the riser. The calculations showed good agreement with experimental findings of both mass flux and pressure profile, but further improvements were proposed and investigated. A parameter study showed that mesh refinement, choice of particle diameter and choice of drag model are crucial when simulating FCC riser flow. The result of the submitted blind test and best result after the parameter study is given in Figure 7.

6.3.2 Reactive flow: Hansen et al. [51] have implemented the isothermal decomposition of ozone in the CFD code FLOTRACS-MP-3D described above. The code is a three dimensional (3D) multiphase computational fluid dynamics code with an Eulerian description of both gas and particle phase. The turbulent motion of the particulate phase is modelled using the kinetic theory for granular flow, and the gas phase turbulence is modelled using a sub-grid-scale model.

The decomposition reaction is studied in a 3D representation of a 0.254m I.D. riser, which has been studied experimentally by Ouyang et al. [49]. These authors obtained profiles of ozone concentration in the 10.85-m high riser by the use of a UV detector system. Furthermore, a pressure drop profile was reported. Comparison between measured and simulated time-averaged ozone concentration at different elevations in the riser shows good agreement. The 3D representation of the reactor geometry gives better predictions of the radial variation in concentration than in a similar 2D simulation, Samuelsberg and Hjertager [53]. Typical results are given in Figure 8.

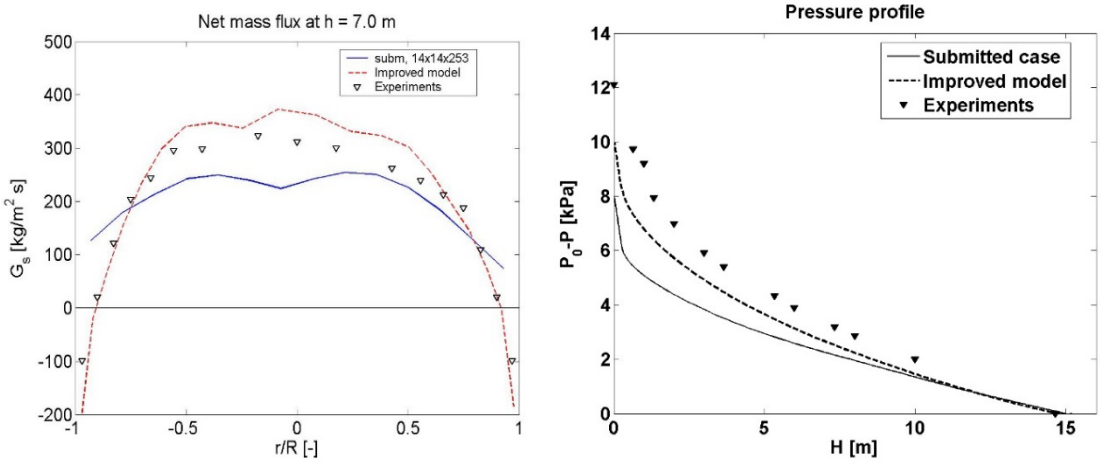

Figure 7: Predicted and measured solids fluxes (left) and pressure profile for blind test and improved cases (right).

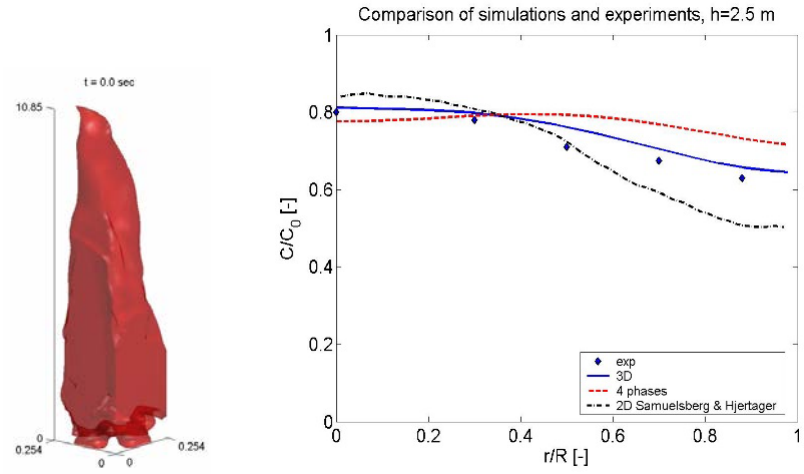

Figure 8: Predicted contours of ozone concentration (iso-surface of $C/C_{inlet} = 0.6$) (left); comparison of measured and predicted radial profile of ozone (right)

7. Summary

The present Paper has presented details of a multi-fluid model for multi-phase flows. Closure laws for both bubble-liquid and solids-gas systems have been exposed. In particular the results using kinetic theory of granular flow (KTGF) have been shown for the solids gas system. Several sub-models are presented including bubble size, chemical reactions as well as heat and mass transfer. Finally, examples of results from bubble-liquid and solids-gas simulations are given.

Acknowledgement

This paper is based on the work that the author and his colleagues have performed in the field of multiphase flow modeling over the last two decades at his two previous affiliations Telemark University College, Porsgrunn, Norway and Aalborg University Esbjerg, Denmark. The author will take this opportunity to thank and acknowledge previous collaborators: Prof., Dr. T. Solberg, Dr. K. Morud, Dr. A. E. Samuelsberg, Dr. E. Manger, Dr. V. Mathiesen, Mr. T. Solbakken, Ms. T. Teppen, Dr. P. Chr. Friberg, Dr. C.H. Ibsen, Dr. N. G. Deen, Dr. K. Granly Hansen, Dr. S. Bove, Dr. J. Madsen, Dr. R. Hansen.

The present paper is based on Hjertager, B.H., 2007. Multi-fluid CFD analysis of chemical reactors, in: Marchisio, D.L., Fox, R.O. (Eds.), *Multiphase Reacting Flows: Modelling and Simulation*. SpringerVerlag, Vienna, Austria. Number 492 in CISM International Centre for Mechanical Sciences, pp. 125–179.

References

[1] Migdal D and Agosta V D 1967 *Appl Mech* **35** pp. 860-5.
[2] Nichols B D, Hirt C W and Hotshkiss R S 1980 *SOLA-VOF: A solution algorithm for transient fluid flow with multiple free boundaries* Report LA-8355 (New Mexico-Los Alamos Sci Lab).
[3] Spalding D B 1985 Computer simulation of two-phase flows with special reference to nuclear reactor systems, in *Computational Techniques in Heat Transfer* ed R W Lewis, K Morgan, J A Johnson,W R Smith (Pineridge Press) pp.1-44.
[4] van der Hoef M A, Van Sint Annaland M and Kuipers J A M 2004 *Chem Eng Sci* **59 (22-23)** pp. 5157–65.
[5] Kataoka I and Serizawa A 1989 *Int. J. Multiphase Flow* **15(5)** pp. 843–55.
[6] Lopez de Bertodano M, Lahey R T and Jones O C 1994 *J. Fluids Eng.* **116** pp. 128-34.
[7] Chahed J, Roig V and Masbernat L 2003 *Int. J. Multiphase Flow* **29** pp. 23-49.

[8] Milelli M 2002 *PhD thesis*: *A numerical analysis of confined turbulent bubble plumes* dissertation eth n. 14799, Swiss Federal Institute of Technology (ETH).
[9] Deen N G, Solberg T and Hjertager B H 2001 *Chem. Eng. Sci*. **56** pp. 6341-49.
[10] Bove S, Solberg T and Hjertager B H 2004 *International J. Chem. Reactor Eng.* **2(1)**.
[11] Sato Y and Sekoguchi K 1975 *Int. J. Multiphase Flow* **2** pp.79-95.
[12] Smagorinsky J 1963 *Month Weather Rev* **91** pp. 99-164.
[13] Bove S 2005 *PhD thesis-Computational fluid dynamics of gas-liquid flows including bubble population balances* (Aalborg Uni. Esbjerg).
[14] Lopez de Bertodano M 1998 *Nucl. Eng. and Design* **179** pp. 65-74.
[15] Drew D A and Passman S L 1999 *Theory of multicomponent fluids* (New York-Springer-Verlag).
[16] Moraga F J, Larreteguy A E, Drew D A and Lahey R T 2003 *Int. J of Multiphase Flow* **29** pp. 655-73.
[17] Lahey R T, Lopez de Bertodano M and Jones O C 1993 *Nucl Eng Design* **141** pp.177-201.
[18] Tomiyama A 2004 *3rd Int Symp on Two-Phase Flow Modelling and Experimentation* (Pisa).
[19] Ishii M and Zuber N 2002 *AIChE J*. **45** pp 707-21.
[20] Tomiyama A, Celata G P, Hosokawa S and Yoshida S 2002 *Int. J. Multiphase Flow* **28** pp. 1497-519.
[21] Ding J and Gidaspow D 1990 *AIChE J.* **36** pp 523-38.
[22] Gidaspow D 1994 *Multiphase flow and fluidization* (London-Ac. Press).
[23] Chapman S and Cowling G 1970 *The mathematical theory of non-uniform gases*. 3 ed. (Cambridge University Press).
[24] Jenkins J T and Savage S B 1983 *J. Fluid Mech.* **130** pp. 187-202.
[25] Lun C K K, Savage S B, Jeffrey D J and Chepurniy N 1984 *J. of Fluid Mech.* **140** pp. 223-56.
[26] Manger E 1996 *PhD thesis-Modelling and simulation of gas/solids flow in curvilinear coordinates* Telemark Inst. of Techn.
[27] Jenkins J T and Mancini F 1987 *J. Appl. Mech.* **54** pp. 27-34.
[28] Mathiesen V, Solberg T, Manger E and B H Hjertager 1996 *5th Int. conf. on circulating fluidized beds* (Beijing)
[29] Gidaspow D, Huilin L and E. Manger 1996 *Proc. of XIXth Int. Cong. of theoretical and applied mechanics*.
[30] Mathiesen V, Solberg T and Hjertager B H 2000 *Int. J. Multiphase flow* **26** pp. 387-419.
[31] Mathiesen V, Solberg T and Hjertager B H 2000 *Powder Techn.* **112** pp.34-45.
[32] Ibsen C H, Solberg T and Hjertager B H 2001 *Ind. & Eng. Chem. Res.* **40 (23)** pp. 5081-86.
[33] Hansen K G, Ibsen C H, Solberg T and Hjertager B H 2003 *Int. J. of Chem. Reactor Eng*. **1(1)**.
[34] Deardorff J W 1971 *J. of Comp. Phys.* **7** pp.120-133.
[35] Bagnold R A 1954 *Proc. Roy. Soc.* **225** pp. 49-63
[36] Ergun S 1952 *Chem. Eng. Prog.* **48 (2)** pp. 89-98.
[37] Wen CY and Yu Y H 1966 *Chem. Eng. Prog. Symp. Ser.* **62** pp. 100-11.
[38] Rowe P N 1961 *Trans of IChemE* **39** pp.175-80.
[39] Gibilaro L G, di Felice R and Waldram S P 1985 *Chem. Eng. Sci*. **40 (10)** pp.1817-23.
[40] Syamlal M and O'Brien T J 1988 *Int. J. Multiphase Flow*, **14 (4)** pp. 473–81.
[41] Johansen S T and Boysan F 1988 *Met. Trans B*, **19B** pp.755-64.
[42] Jakobsen H A 1993 *Dr. ing. Thesis-On the modelling and simulation of bubble column reactors using a two-fluid Model* (Trondheim-Norwegian Institute of Technology).
[43] Calderbank P H 1958 *Trans of IChemE*, **36** pp.443-63.
[44] Cook T L and Harlow F H 1986 *Int. J. Multiphase Flow*, **12** pp. 35-61.
[45] Marchisio D L 2007 *Multiphase Reacting Flows: Modelling and Simulation* (Vienna SpringerVerlag) Number 492 in CISM Int. Centre for Mechanical Sciences ed R O Fox pp. 125–79.
[46] Samuelsberg A and Hjertager B H 1996 *5th Int. conf. on circulating fluidized beds* (Beijing).
[47] D Geldart ed 1986 *Gas fluidization technology* (Chichester- John Wiley & Sons)

[48] Trägårdh C 1988 *Bioreactor Fluid Dynamics* (Elsevier Appl Sci Publ.) pp. 117-34.
[49] Ouyang S, Lin J and Potter O E 1993 *Powder Techn.* **75** pp.73-78.
[50] van den Hengel E I V, Deen N G and Kuipers J A M 2005 *Ind. Eng. Chem. Res.* 44 (14) pp. 5233-45.
[51] Deen N G, Solberg T and Hjertager B H 2003 *The Can. J. Chem. Eng.* **80(4)** pp. 638-52.
[52] Hansen K G, Solberg T and Hjertager B H 2004 *Chem. Eng. Sci.* **59(22-23)** pp.5217-24.
[53] Samuelsberg A and Hjertager B H 1995 *Adv. in Multiphase Flow* pp. 679-88.